MODELING OF COMBUSION PROCESSES OF STICK PROPELLANTS
VIA COMBINED EULERIAN-LAGRANGIAN APPROACH.

K. K. Kuo, K. C. Hsieh, M. M. Athavale
Department of Mechanical Engineering
The Pennsylvania State University
University Park, Pennsylvania

This research is motivated by the improved ballistic performance of large-caliber guns using stick propellant charges. A comprehensive theoretical model for predicting the flame-spreading, combustion , and grain deformation phenomena of long unslotted stick propellants is presented. The formulation is based upon a combined Eulerian-Lagrangian approach to simulate special characteristics of the two-phase combustion processes in a cartridge loaded with a bundle of sticks. The model considers five separate regions consisting of the internal perforation, the solid phase , the external interstitial gas phase, and two lumped parameter regions at either end of the stick bundle. For the external gas-phase region, a set of transient one-dimensional fluid-dynamic equations using the Eulerian approach is obtained; governing equations for the stick propellants are formulated using the Lagrangian approach. The motion of a representative stick is derived by considering the forces acting on the entire propellant stick. The instantaneous temperature and stress fields in the stick propellant are modeled by considering the transient axisymmetric heat-conduction equation and dynamic structural analysis. For the internal perforation region, a set of one-dimensional transient fluid-dynamic equations is formulated with a coordinate system attached to the moving stick. Major distinctions between the present and the conventional formulations for interior ballistic simulation are delineated.

I. Introduction

Recently, there has been an increasing interest in the use of stick propellant charges in large-caliber gun systems. Stick propellants offer many advantages over conventional randomly packed multi-perforated granular propellant charges. The regular geometry of stick propellants allows a higher loading density, flexibility in charge design, and easier charge loading. The higher charge density is preferable for low vulnerability ammunition (LOVA) propellants, which require a higher propellant mass to produce an equivalent performance. It has been observed by Robbins et al. (1,2) that flow resistance through the charge of a stick propellant bundle is lower than that through packed beds of granular propellants, thus enabling faster and more reproducible flame spreading through the stick propellant charge. The lower flow resistance also reduces considerably the phenomena of high pressure gradients and severe pressure waves in the gun tube, as indicated by Minor (3).

A number of studies (1-10) on various aspects of stick propellant combustion have been reported to date. The NOVA code, developed by Gough (11,12) for ballistic performance of granular charges, was used with some modifications (1,4) to predict the performance of a stick propellant charge. Results obtained were in good agreement with experimental data for multiperforated granular NACO propellants and single-perforated slotted stick bundles (1). However, the same is not true for the case of single-perforated, unslotted stick propellants.

The structure mechanics consideration in the continuum modeling of unslotted stick charge combustion of the modified NOVA code (4) is rather crude, due to the application of a steady-state relationship between radial and hoop stresses and internal and external pressures. Although pressure distributions in the internal perforation were calculated, only the external pressure was used in evaluating the axial stress component, which is in turn related to the intra-granular stress. Grain deformation and fracture of unslotted long sticks are mainly due to the radial expansion and attainment of a critical hoop stress.

Rupture of stick propellants during combustion in a gun barrel was observed by Robbins and Horst (2). Grain fracture can lead to high peak pressures due to increase in total burning surface area. The pressure difference across the web of a stick propellant can cause the grain to deform prior to fracture and alter the flow-channel width and the distance between opposite burning surfaces, thereby changing the combustion process. Hence, the prediction of grain deformation and rupture should be given due importance in the overall interior ballistic cycle.

The proposed model is based on a relatively new method, previously applied to two-phase reacting flow problems such as spray combustion of liquid droplets (14). In the separated-flow approach, the continuous phase (gas phase) is treated by a Eulerian approach, while the condensed phase media (stick propellants) are divided into several representative groups and tracked, using a Lagrangian approach, as they move in the continuous phase. The interstitial gas-phase region in the present problem is treated in a similar fashion to the continuous phase in spray combustion, while the internal gas-phase regions in the grain perforations are treated separately. The flame-spreading and combustion phenomena inside the perforation are similar to those in a cylindrical side-burning rocket motor grain. The ignition transient analysis developed by Peretz et al. (15) is therefore adapted to model the flame spreading and combustion processes in the perforation. This two-phase separated flow approach is convenient because the

stick propellants have identical dimensions and symmetry about their own axes as well as a central axis. The number of representative sticks in a stick propellant bundle is relatively low, therefore making it possible to study some of the detailed flow and combustion phenomena of these representative stick propellant grains.

All of the gun interior ballistic codes and analyses developed so far do not consider the distribution of chemical species (16-18). The heat release is assumed to occur at the same location as that of pyrolysis of the propellant. However, for LOVA or other types of modern propellants, some chemical species could be pyrolyzed from the propellant surface, be carried by the flow during the ignition transient interval, and then react at some downstream location. Therefore, in general, the heat release could occur at a different position than the site of initial pyrolysis. These complicated phenomena, which were simplified in previous analyses, are included in the present model.

Objectives of the current research are to formulate a combined Eulerian-Lagrangian model for the combustion of a bundle of stick propellants inside a gun chamber. It is intended to cover many aspects of realistic simulation of stick propellant combustion characteristics so that the model is capable of predicting the phenomena of ignition, flame spreading, and combustion of stick propellants. Development of the model is also intended to help explain the experimental observations from test firings being conducted by the authors in a simulated gun system. The data to be obtained will be used for model validation.

II. Method of Approach

1. Physical Model

Figure 1 shows a bundle of stick propellants loaded in the combustion chamber of a gun. For the present model, only unslotted long stick propellant grains are considered. In the theoretical formulation, the combustion chamber is divided into five separate regions: 1) lumped parameter region near the base pad; 2) internal perforation region; 3) external interstitial gas-phase region; 4) solid propellant region; and 5) lumped parameter region near the base of the projectile. Although the solid propellant region consists of many stick propellants, only a few representative sticks are required to be modeled due to the similarity of the sticks in the same family. Each region has a separate set of governing equations which are coupled through various boundary conditions. The erosive burning of the stick propellants under cross-flow conditions is also taken into account. Since fracture phenomena of stick propellants under dynamic loading conditions are under investigation, the present model is limited to the time period before one or more stick propellants rupture as a result of high pressure differential across the web of the stick propellant. After the onset of rupture, a stick propellant could become partially slotted, broken, and/or highly deformed. It is then difficult to distinguish the internal versus external surface. These phenomena are beyond the scope of the present model.

2. Mathematical Formulation
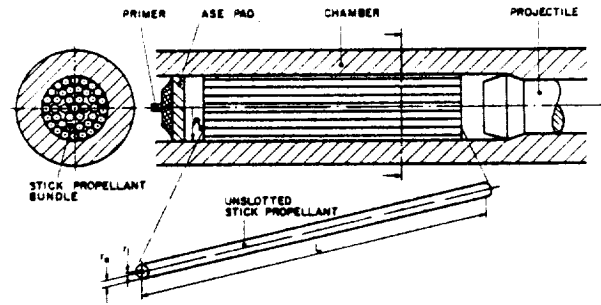
A. Basic Assumptions:

Fig.1 Stick propellant Charge in a Cartridge of a Large Caliber Gun.

(1) All the stick propellants have the same initial geometry and physical conditions. Furthermore, it is possible to divide the stick bundle into a few families so that the calculations can be performed for only a few representative sticks. To simplify the mathematical formulation, the combustion of sticks in a bundle is represented by a single stick. The mathematical format can be readily extended to multiple families of sticks.

(2) Assumptions used in the gas-phase regions are:

a. no body forces;
b. bulk viscosity μ' is negligible;
c. Soret and Dufour effects are negligible;
d. gases obey Noble-Abel equation of state;
e. all binary diffusion coefficients are equal;
f. Fick's law of diffusion is valid;
g. flow is one-dimensional transient (properties are uniform in r and θ directions);
h. total flow area in the external gas-phase region is assumed to be ϕA [Dupuit Forchheimer hypothesis (19)]; and
i. turbulence correlations of flow properties in the axial direction are considered negligible in comparison with the product of their mean flow properties. However, turbulence effects in the transverse direction are embedded in the empirical correlations.

(3) Assumptions used for the solid propellant are:

a. burning in the inner and outer surfaces of a stick is axisymmetric;
b. density of the solid is constant;
c. any subsurface heat release occurs very close to the surface and therefore can be lumped onto the surface;
d. torsion and rotation are negligible;
e. each stick propellant is locally axisymmetric;
f. burning at the end surfaces is uniform;
g. end surfaces are perpendicular to the axis of the stick; and
h. propellant material behaves as a linear viscoelastic material in shear and elastic material in bulk deformation.

B. Overall Structure of the Mathematical Model

Overall Model

External gas phase
- Basic assumptions
- Governing equations (based upon Eulerian coordinate system)
  - Transport equations for flow variables ρ_{ge}, u_{ge}, $(Y_i)_e$, T_{ge}
    - Thermal properties
    - Gas-phase reaction kinetics
    - Transport properties
  - Initial and boundary conditions
- Empirical correlations
  - Propellant burning rate
  - Heat transfer between gases and solid surfaces
  - Viscous drags between gases and solid surfaces

Solid phase
- Governing equations (based upon Lagrangian coordinate fixed to the moving stick)
  - Mass, momentum equations for M and u_s
  - Dynamic structural analysis for grain deformation
    - Constitutive relationship
    - Mechanical properties
  - Energy equation
    - Conduction equation
    - Radiation transport equations
  - Initial and boundary conditions
- Empirical correlations and constants
  - Ignition criterion
  - Thermal properties
  - Burning rate law

Internal gas phase
- Basic assumptions
- Governing equations (based upon Eulerian coordinate fixed to the stick propellant)
  - Transport equations for flow variables ρ_{gi}, V_{gi}, $(Y_i)_i$, T_{gi}
    - Thermal properties
    - Gas-phase reaction kinetics
    - Transport properties
  - Equation of state
  - Initial and boundary conditions
- Empirical correlations
  - Propellant burning rate
  - Convective heat transfer coefficient
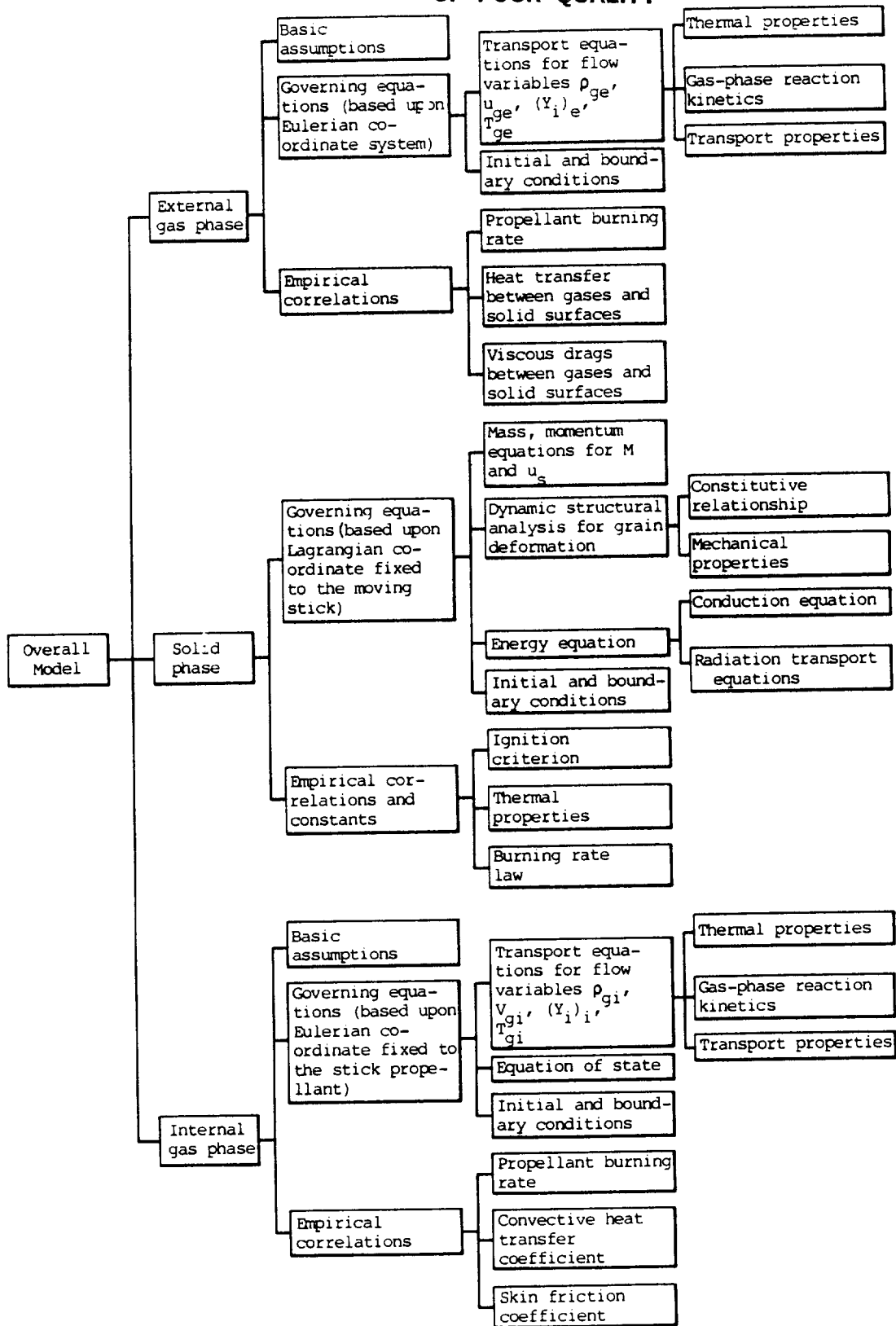 - Skin friction coefficient

Fig.2 Overall Structure of the Theoretical Model

In order to give an overview of the structure of the mathematical model, Fig. 2 was constructed. It shows the major components and subcomponents of the formulation for each region in the physical model. To simplify the diagram, the cross-coupling lines between each region are not shown. However, it is important to note that the physicochemical processes in these regions are closely coupled. Mathematical representations of each component and subcomponent are given in the following sections.

C. Governing Equations for the External Gas-Phase Region

The external gas-phase region occupies the whole interstitial space in the cartridge, excluding the shaded region shown in Fig. 3. By using the control volume analysis (reference to Eulerian coordinate), the following governing equations are obtained.
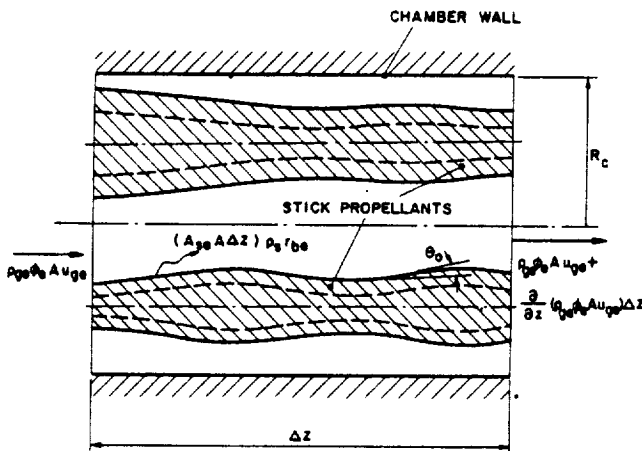
Fig.3 Schematic Diagram Showing the Mass Fluxes Entering and Leaving the External Gas-Phase Region (Unshaded and Multiply Connected Region).

Continuity Equation:

$$\frac{\partial(\rho_{ge}\phi_e)}{\partial t} + \frac{\partial(\rho_{ge}\phi_e u_{ge})}{\partial z} = \frac{2}{R_c^2}\sum_{j=1}^{N} r_{o_j}\rho_s r_{be} \quad (1)$$

where ϕ_e is the void fraction of the external gas-phase region and is defined as

$$\phi_e = 1 - \frac{1}{R_c^2}\sum_{j=1}^{N} r_{o_j}^2 \quad (2)$$

Momentum Equation:

$$\frac{\partial(\rho_{ge}\phi_e u_{ge})}{\partial t} + \frac{\partial(\rho_{ge}\phi_e u_{ge}^2)}{\partial z} =$$

$$- \phi_e\frac{\partial P_e}{\partial z} + \frac{\sum_{j=1}^{N} r_{o_j}}{R_c^2}\rho_s r_{be}(u_s - V_{ge}\sin\theta_o)$$

$$- \frac{\sum_{j=1}^{N} r_{o_j}}{R_c^2}\underbrace{(D_{ve} + \frac{\partial}{\partial z}(\dots\phi_e\frac{\partial u_{ge}}{\partial z})}_{small} - \frac{2\tau_w}{R_c} \quad (3)$$

where $V_{ge}\sin\theta_o$ is the horizontal component of the gasification velocity normal to the solid propellant surface. The second term in the right-hand side represents the momentum transfer from solid propellant to the external gas-phase region due to burning.

Energy Equation:

$$\frac{\partial(\rho_{ge}\phi_e E_e)}{\partial t} + \frac{\partial(\rho_{ge}u_{ge}\phi_e E_e)}{\partial z} + \frac{\partial(P_e u_{ge}\phi_e)}{\partial z}$$

$$= \frac{2\sum_{j=1}^{N} r_{o_j}}{R_c^2}\rho_s r_{be}\left[\sum_{i=1}^{M} Y_{ie}h_{ie} + \frac{1}{2}\left(\frac{\rho_s r_{be}}{\rho_{ge}}\sin\theta_o + u_s\right)^2\right]$$

$$- \frac{2\sum_{j=1}^{N} r_{o_j}}{R_c^2}\bar{h}_{te}(T_{ge} - T_{se}) - \frac{2\sum_{j=1}^{N} r_{o_j}}{R_c^2}D_{ve}u_s - P_e\frac{\partial\phi_e}{\partial t}$$

$$+ \underbrace{\frac{\partial}{\partial z}(k_{ge}\phi_e\frac{\partial T_{ge}}{\partial z})}_{small} + \underbrace{\frac{4}{3}\frac{\partial}{\partial z}(\dots_e\phi_{ge}\phi_e\frac{\partial u_{ge}}{\partial z})}_{small} - 2\dot{Q}_w/R_c \quad (4)$$

where h_i is the enthalpy of the ith species defined as

$$h_i = \Delta h_{f,i}^o + \int_{T_o}^{T_s} C_{p,i}dT \quad (5)$$

and E_e is the sum of the internal and kinetic energy of the gas phase in the control volume. The energy transfer due to molecular species diffusion has been neglected because of a high degree of turbulence.

Species Continuity Equation:

$$\frac{\partial(\phi_e\rho_{ge}Y_{ie})}{\partial t} + \frac{\partial(\phi_e\rho_{ge}u_{ge}Y_{ie})}{\partial z} =$$

$$\frac{\partial}{\partial z}(\phi_e\rho_{ge}D\frac{\partial Y_{ie}}{\partial z}) + (\dot{\omega}_i)_e \quad (6)$$

where the source term $(\dot{\omega}_i)_e$ consists of contributions cause by surface pyrolysis and gas-phase reactions, i.e.

$$(\dot{\omega}_i)_e = (\dot{\omega}_i)_{e,s} + (\dot{\omega}_i)_{e,g} \quad (7)$$

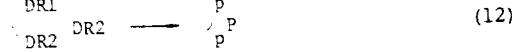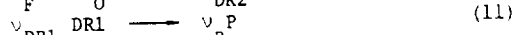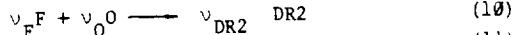where the surface pyrolysis part can be expressed as

$$(\dot{\omega}_i)_{e,s} = r_{be}\rho_s A_{se}Y_{is}^* \quad (8)$$

where Y_{is}^* represents the mass fraction of the ith species pyrolyzed from the solid propellant before mixing with ambient gases. Following the flame model proposed by Wu et al. (20) in their study of erosive burning of homogeneous propellants, the solid propellant pyrolyzes into three groups of species:

Solid Propellant ——— Oxidizer-rich gases (O)
+
Fuel-rich gases (F)
+
First group of species
with delayed reaction (DF) (9)

Under low cross flow conditions, the flame structure adjacent to a burning homogeneous propellant

184

surface exposed to a large cavity can be assumed to have three stages, as shown in Fig. 4a. This flame structure is based upon the erosive burning study in a rocket motor by Wu et al. (20). In the case of large-caliber guns densely loaded with stick propellants, the void spaces adjacent to burning surfaces are relatively small, and the species pyrolyzed from the surface can be entrained by the high-velocity gases flowing along the axis. The heat release in the final flame generated by the chemical reaction of pyrolyzed species from a specific location occurs at a downstream location, as shown in Fig. 4b. To determine the gas phase reaction rate and heat-release rate, the same chemical reaction mechanism, proposed in Ref. 20, is adopted. This mechanism can be represented by three overall chemical steps:

$$\nu_F F + \nu_O O \longrightarrow \nu_{DR2} \ DR2 \tag{10}$$
$$\nu_{DR1} \ DR1 \longrightarrow \nu_P P \tag{11}$$
$$\nu_{DR2} \ DR2 \longrightarrow \nu_P P \tag{12}$$

Oxidizer-rich gases (O) can be regarded as NO_2 species, fuel-rich gases (F) as a group of aldehydes (CH_2O), and other species generated by surface pyrolysis as one group of delayed reaction species (DR1). Based upon the work of Fifer (21) and Kubota (22), chemical reaction in the Fizz zone is largely due to the reaction involving reduction of NO_2 to NO. After the delay in the dark zone, the reactions in the final flame can be assumed to occur at high activation energies, associated with reactions (11) and (12) to form the final products from DR1 and the second group of delayed reaction species (DR2). In the dark and final flame zones, chemical reactions result in oxidation of CO, and perhaps some H_2 by NO. More detailed discussions of kinetic parameters and mechanisms are given in Ref. 20-22.

It is useful to point out that the chemical reaction mechanism proposed in Ref. 20 can be followed for highly turbulent cross-flow situations. The O and F species pyrolyzed from the solid propellant originate at the same place, and flow together in a torturous path to form DR2 and final products (P). The delayed reaction species of DR1 can also be considered to flow together in the process to form product species P. Gases in the cross-flow can transfer heat to these species and alter the delay times required to form product species P. The stoichiometric coefficients ν_F, ν_O, ν_{DR1}, and ν_{DR2} are therefore functions of propellant ingredients only. The method for calculating these parameters is based upon the original molecular structure of the propellant and is discussed in Ref. 20.

In Ref. 20, the rate of production of species "i" was based upon the chemical reaction rate as well as the eddy-break-up rate (23) controlled by the turbulence intensity and concentration gradient. Turbulence intensity is so high in the gun situation because of base-pad ignition and combustion of propellants that the species diffusion term can be regarded as extremely short. Therefore, the rate of consumption or production of species is determined solely from chemical reaction time.

The rate of chemical reaction of species F, DR1, O, and DR2 are given below in the same form as in Ref. 20.

$$(\dot{\omega}_F)_{e,g} = - A_F \ \exp(-E_{a,F}/R_u T_{ge}) \rho_{ge}^2 (Y_F Y_O)_e / W_F \tag{13}$$

$$(\dot{\omega}_{DR1})_{e,g} = - A_{DR1} \ \exp(-E_{a,DR1}/R_u T_{ge}) \rho_{ge}^2 Y_{DR1_e}^2 / W_{DR1} \tag{14}$$

$$(\dot{\omega}_O)_{e,g} = (\dot{\omega}_F)_{e,g} \frac{\nu_O W_O}{\nu_F W_F} \tag{15}$$

$$(\dot{\omega}_{DR2})_{e,g} = - A_{DR2} \ \exp(-E_{a,DR2}/R_u T_{ge}) \rho_{ge}^2 Y_{DR2_e}^2 / W_{DR2}$$
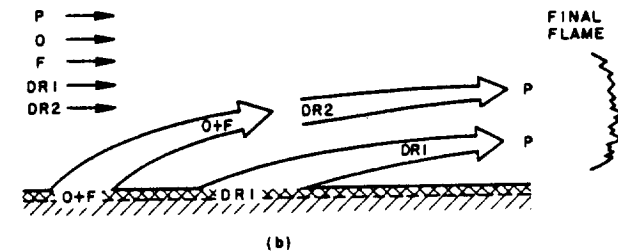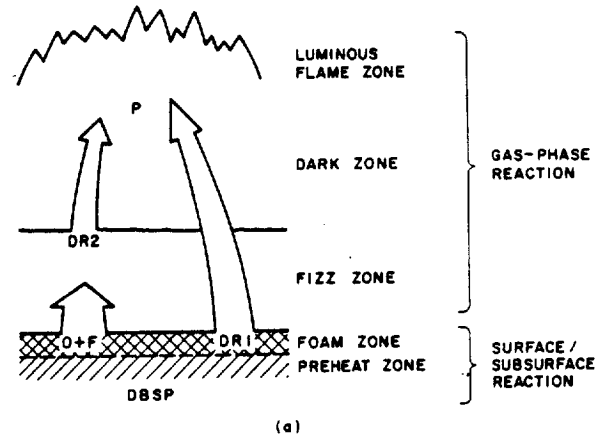$$- (1 + \nu_O W_O / \nu_F W_F)(\dot{\omega}_F)_{e,g} \tag{16}$$

Fig.4 Flame Structure of a Homogeneous Solid Propellant (a) Two-dimensional Structure under Low Cross-Flow Velocities, (b) Distorted Flame under Extremely High Cross-Flow Velocities (Nearly One-Dimensional Structure).

Equation of State:

The Noble-Abel dense gas law is used.

$$P_e (\frac{1}{\rho_{ge}} - b) = RT_{ge} \tag{17}$$

The initial and boundary conditions as well as empirical correlations for the external gas-phase region are given in a later section.

D. Governing Equations for the Stick Propellant

The following governing equations for a representative stick are derived based upon the Lagrangian coordinate.

1) Mass and Momentum Equations:

The instantaneous mass of the representative stick can be calculated from

185

$$M_s(t) \equiv \int_{-L(t)/2}^{L(t)/2} \rho_s \pi [r_o^2(t,\xi) - r_i^2(t,\xi)] d\xi \quad (18)$$

The instantaneous values of stick propellant length, $L(t)$, and the local inner and outer radii, $r_i(t,\xi)$ and $r_o(t,\xi)$, are determined by integrating the following first order differential equations.

$$\frac{\partial r_i(t,\xi)}{\partial t} = r_{bi}(t,\xi) + V_{sr_i}(t,\xi) \quad (19)$$

$$\frac{\partial r_o(t,\xi)}{\partial t} = -r_{be}(t,\xi) + V_{sr_o}(t,\xi) \quad (20)$$

$$\frac{dL(t)}{dt} = -r_{b_{LB}}(t) - r_{b_{RB}}(t) + V_{SRB}(t) - V_{SLB}(t) \quad (21)$$

where V_{sr_i} and V_{sr_o} represent the radial velocities of the inner and outer surfaces of the stick propellant due to mechanical deformation with respect to the centerline of the stick. V_{SRB} and V_{SLB} represent the rate of mechanical deformation of the right and left boundary surfaces with respect to the geometric center of the stick. The equation of motion is formulated according to the following momentum balance principle.

$$\frac{d(M_s u_s)}{dt} = \Sigma F_\xi + \text{(net rate of momentum flux flowing into the control volume encompassing the stick propellant)} \quad (22)$$

which gives (see Fig. 5)

$$\frac{d}{dt}(M_s u_s) = -2\pi \int_{-L/2}^{L/2} [P_i \sin\theta_i - \tau_i \cos\theta_i] r_i d\xi - (F_{pp} + F_{pw})$$

$$+ 2\pi \int_{-L/2}^{L/2} [P_o \sin\theta_o + \tau_o \cos\theta_o] r_o d\xi$$

$$+ 2\pi \rho_s^2 \int_{-L/2}^{L/2} \left[\frac{r_{be}^2 r_o \sin\theta_o}{\rho_{ge}} - \frac{r_{bi}^2 r_i \sin\theta_i}{\rho_{gi}} \right] d\xi$$

$$- \pi \left[(r_o^2 - r_i^2)(P + \frac{\rho_s^2 r_b^2}{\rho_g}) \right]_{\xi=\frac{L}{2}}$$

$$+ \pi \left[(r_o^2 - r_i^2)(P + \frac{\rho_s^2 r_b^2}{\rho_g}) \right]_{\xi=-\frac{L}{2}} \quad (23)$$

where F_{pw} represents the net force acting between the stick propellant and chamber wall, and F_{pp} is the force between adjacent propellants.
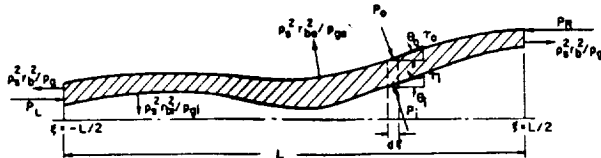

Fig.5 Momentum fluxes and Pressure Forces Acting on the Entire Surface of a Single Perforated Stick Propellant.

2) Transient Heat Conduction Equation:

To determine the instantaneous temperature distribution in the stick propellant, a heat conduction equation must be considered. The equation, which takes into account the subsurface radiation absorption for translucent propellants, has the following form.

$$\rho_s \frac{\partial(C_s T_s)}{\partial t} = \frac{1}{r}\frac{\partial}{\partial r}(rk_s\frac{\partial T_s}{\partial r}) + \frac{\partial}{\partial \xi}(k_s\frac{\partial T_s}{\partial \xi})^{\overset{small}{}}$$

$$+ a\left[(I_r - E_b) + (J_r - E_b)\right] \quad (24)$$

where E_b is the black-body emissive power evaluated as σT_s^4, and "a" represents the flux absorption coefficient of the propellant. This equation is based upon a two-flux model which assumes that the radiation fluxes are dominant in the radial directions (inward and outward). The source terms represent the net rate of energy absorbed due to radiant energy fluxes. The outward and inward radiant fluxes, I_r and J_r, can be determined from the following flux-transport equations.

$$\frac{d(rI_r)}{dr} = -(s+a)rI_r + arE_b + J_r + \frac{1}{2}sr(I_r + J_r) \quad (25)$$

$$\frac{d(rJ_r)}{dr} = (s+a)rJ_r - arE_b + J_r - \frac{1}{2}sr(I_r + J_r) \quad (26)$$

These two equations were used by Gosman and Lockwood.(24)

3) Dynamic Structural Analysis

As a result of the different ignition and flame spreading processes occuring in the internal perforation and external gas-phase regions, a pressure differential exists across the web of a representative stick. A finite element analysis is needed to compute the resulting transient viscoelastic deformation of the stick propellant and to predict the attainment of a critical condition for grain fracture. Regression of the boundary as a result of pyrolysis and burning should also be taken into account. Furthermore, the mechanical properties of the stick propellant must be specified.

The propellant material can be considered as linear viscoelastic in shear and elastic in bulk deformation. This is a commonly accepted practice for solid propellant (25, 26). The elastic bulk behavior is assumed to follow

$$\sigma_i^i = 3K\epsilon_i^i \quad (27)$$

where K is the bulk modulus. The deviatoric behavior is taken as

$$S_{ij} = \int_0^t G_1(t-t') \frac{\partial e_{ij}(t')}{\partial t'} dt' \quad (28)$$

where the shear relaxation modulus $G_1(t)$ is assumed to be of the form

$$G_1(t) = G_\infty + (G_0 - G_\infty)e^{-\beta t} \quad (29)$$

186

where G_∞ is the long-time shear modulus, G_0 is the short-time shear modulus, and β is the decay constant. Since a closed-form solution for the axisymmetric dynamic problem is not possible, a well-established finite element code "HONDO-II" (26) is employed for computations of grain deformation. The code utilizes the principle of virtual work for the solution. It states that at all the points along the path of motion, the differential virtual work, $\delta\pi$, must vanish for all variations δx_k satisfying the imposed displacement boundary conditions (26). $\delta\pi$ is defined as

$$\delta\pi = \int_V \rho\ddot{x}^k \delta x_k dv + \int_V \sigma^{km}\delta x_{k,m} dv - \int_V \rho f^k \delta x_k dv$$
$$- \oint_S \tau^k \delta x_k ds \qquad (30)$$

where τ^k is surface traction and σ^{km} is Cauchy stress tensor. The stick propellant is divided into a number of elements over the cross-sectional area of the web. The HONDO-II code uses four mode bilinear isoparametric elements. The basic equation of motion, viz., the minimization of virtual work, is then considered for each of the nodes in the stick propellant. Thus, the equation of motion for a node becomes

$$\delta\pi = \sum_{n=1}^N \left\{ \int_{V_n} \rho\ddot{x}^k \theta_{\sim k}^\ell \, dv + \int_{V_n} \sigma^{km} \theta_{\sim k,m}^\ell dv \right.$$
$$\left. - \int_{V_n} \rho f^k \theta_{\sim k}^\ell dv - \oint_{S_n} \tau^k \theta_{\sim k}^\ell ds \right\} = 0 \qquad (31)$$

where $\theta_{\sim k}^\ell = [\phi_k^1, \phi_k^2, \phi_k^3, \phi_k^4]\Big|_{V_n}$

and ϕ_k^ℓ are the bilinear interpolation functions. In Eq. (31), N is the total number of elements surrounding the node in question. The calculations are carried out on an element-by-element process to get the final equations of motion. The time integration of these equations gives the positions of nodes at the new time step. A central difference method is used for time integration in the HONDO-II code.

E. Governing Equations for the Internal Gas-Phase Region

Conservation equations for the control volume in the perforation of a stick propellant are similar to those given in Ref. 15.

Continuity Equation:

$$\frac{\partial(\rho_{gi} A_p)}{\partial t} + \frac{\partial(\rho_{gi} A_p V_{gi})}{\partial\xi} = r_{bi}\rho_s P_b \qquad (32)$$

where ξ is the distance measured from the center of the stick, and V_{gi} is the velocity of the gas relative to the velocity of the stick propellant. V_{gi} is related to the absolute velocity u_{gi} by

$$V_{gi} = u_{gi} - u_s \qquad (33)$$

Momentum Conservation Equation:

$$\frac{\partial(\rho_{gi} V_{gi} A_p)}{\partial t} + \frac{\partial(\rho_{gi} V_{gi}^2 A_p)}{\partial\xi} = - A_p \frac{\partial P_i}{\partial\xi} - D_{Vi} P_b$$
$$+ \underbrace{\frac{\partial(\tau_{\xi\xi} A_p)}{\partial\xi}}_{small} + \underbrace{\frac{\rho_s^2 r_{bi}^2 A_p}{\rho_{gi} \partial\xi}}_{small} \qquad (34)$$

Energy Conservation Equation:

The energy conservation equation written for the stored total energy (internal and kinetic) per unit mass, E_{gi}, is

$$\frac{\partial(\rho_{gi} A_p E_{gi})}{\partial t} + \frac{\partial(\rho_{gi} A_p V_{gi} E_{gi})}{\partial\xi} = \frac{\partial}{\partial\xi}\underbrace{(k_{gi} A_p \frac{\partial T_{gi}}{\partial\xi})}_{small}$$
$$- \frac{\partial(A_p P_i V_{gi})}{\partial\xi} - \frac{\partial}{\partial\xi}(\tau_{\xi\xi} A_p V_{gi}) - \bar{h}_{ti}(T_{gi} - T_{si}) P_b$$
$$+ \rho_s r_{bi} P_b \left[\sum_{j=1}^M Y_j^* h_j(T_{si}) \right]_i \qquad (35)$$

Species Continuity Equation:

The species continuity equation for the internal gas-phase is similar to that for the external gas-phase, with the void fraction taken as one and the absolute velocity replaced by the relative velocity.

$$\frac{\partial[\rho_{gi}(Y_i)_i]}{\partial t} + \frac{\partial[\rho_{gi} V_{gi}(Y_i)_i]}{\partial\xi}$$
$$= \frac{\partial}{\partial\xi}\left[\underbrace{\rho_{gi} D \frac{\partial(Y_i)_i}{\partial\xi}}_{small}\right] + (\dot{\omega}_i)_i \qquad (36)$$

where the source term $(\dot{\omega}_i)_i$, similar to $(\dot{\omega}_i)_e$ in Eq. (7), consists of contributions due to surface pyrolysis and gas-phase reactions. The flame model for the internal gas-phase region is the same as that given earlier for the external gas-phase region.

F. Heat Losses to the Walls of the Combustion Chamber

In order to consider heat losses from the combustion zone to the cartridge chamber, the gun tube, and the projectile, temperature profiles in these metal components are required. For a test rig with a blowout diphragm and short barrel, the transient ignition and combustion phenomena occur in an extremely short time interval and the heat loss to the surrounding walls can be considered negligible. However, if the simulation is made for the full ballistic cycle occurring in a long gun barrel, the loss to the walls must be considered. The heat conduction to the gun tube can be given as

$$\rho_w \frac{\partial(C_w T_w)}{\partial t} = \frac{\partial}{\partial z}(k_w \frac{\partial T_w}{\partial z}) + \frac{1}{r}\frac{\partial}{\partial r}(k_w r \frac{\partial T_w}{\partial r}) \qquad (37)$$

The transient heat conduction equation for the wall on the breech end will follow the one-dimensional form:

$$\rho_w \frac{\partial(C_w T_w)}{\partial t} = \frac{\partial}{\partial z}\left(k_w \frac{\partial T_w}{\partial z} \right) \tag{38}$$

The equation for the projectile is:

$$\rho_w \frac{D(C_w T_w)}{Dt} = \frac{\partial}{\partial z}\left(k_w \frac{\partial T_w}{\partial z} \right) \tag{39}$$

The solution of these equations are coupled to the external gas-phase region through the boundary conditions on the wall surfaces.

G. Initial and Boundary Conditions

For each of the above governig equations, there is a set of boundary and/or initial conditions required to complete the formulation. The initial conditions can be specified readily, since the gas and stick propellant velocities are zero and the pressure and temperature of gas in the cartridge is at room conditions. The stick propellant charge with known geometry and its surrounding chamber are also at room temperature. Since the amount of air in the initial loading of the cartridge is extremely small in comparison with the gases generated from combustion, it can be treated as any one of the five species discussed above. in view of the fact that air contains oxygen, it is treated as oxidizer-rich gas (O).

A number of important boundary conditions are given in the following.

1). Boundary Conditions for the stick Propellant

The boundary condition for Eq.(24) at outer surface of the stick propellant can be written as

$$k_s \frac{\partial T_s}{\partial r}\Big|_{r_o}^{-} = \bar{h}_c(T_{ge}-T_{se}) + \rho_s r_{be}(Q_s)_{chem} + (\dot{q}_{rad})_e$$
$$+ \rho_s r_{be}(C_s-C_{pge})T_{se} + (\dot{Q}_{CPIP})_e \tag{40}$$

where $(\dot{Q}_{CPIP})_e$ represents the rate of energy input due the deposit of condensed phase igniter products onto the external surface and $(\dot{q}_{rad})_e$ the net radiative heat flux to the surface can be expressed as

$$(\dot{q}_{rad})_e = J_r\Big|_{r=r_o^+} + \varepsilon_s I_r\Big|_{r=r_o^-} - \varepsilon_s E_b T_{se} \tag{41}$$

Similarly, the boundary condition for the inner surface of the stick propellant can be written as

$$-k_s \frac{\partial T_s}{\partial r}\Big|_{r_i}^{+} = \bar{h}_c(T_{gi}-T_{si}) + \rho_s r_{bi}(Q_s)_{chem} + (\dot{q}_{rad})_i$$
$$+ \rho_s r_{bi}(C_s-C_{pgi})T_{si} + (\dot{Q}_{CPIP})_i \tag{42}$$

where

$$(\dot{q}_{rad})_i = I_r\Big|_{r=r_i^-} + \varepsilon_s J_r\Big|_{r=r_i^+} - \varepsilon_s E_b T_{si} \tag{43}$$

The pressure distributions along the internal perforation and external interstitial regions solved from the gas-phase equations are used as boundary conditions for the solid-phase dynamic structral analysis.

2). Boundary Conditions for the External and Internal Gas-Phase Regions

For simplicity in expressing the boundary treatments, only one representative group of stick propellants is considered, then each stick propellant has the identical instantaneous velocity and length. Therefore, the governing equations for the left lumped-parameter region (see Fig. 6) or called left control volume (LCV) can be readily derived and written as follows.

Mass balance:

$$\frac{d\rho_{g_{LCV}}}{dt} = - \rho_{g_{LCV}} \frac{(u_s+r_{b_{LB}})}{z_L}$$
$$+ \frac{\left[1-\psi_s - \frac{\rho_{g_{LCV}}}{\rho_{ign}}\phi_{LCV}\right]\dot{m}_{ign}-\dot{m}_{oute}-\dot{m}_{outi}}{\pi R_c^2 \phi_{LCV} z_L} \tag{44}$$

where z_L is the length of the left lumped-parameter region and can be calculated from

$$z_L = z_{L_o} + \int_0^t (u_s+r_{b_{LB}})dt + \int_0^t \frac{\dot{m}_{ign}}{\pi R_c^2 \rho_{ign}} dt \tag{45}$$

and

$$\dot{m}_{oute} = \phi_e \pi R_c^2 \rho_{pg}[u_{ge} - (u_s+r_{b_{LB}})]\Big|_{\xi=-L/2} \tag{46}$$

$$\dot{m}_{outi} = N\pi r_i^2 \rho_{gi}[u_{gi}-(u_s+r_{b_{LB}})]\Big|_{\xi=-L/2} \tag{47}$$

Momentum balance:

$$\frac{du_{g_{LCV}}}{dt} = \frac{1}{M_{g_{LCV}}}\left\{ u_{g_{LCV}}[\dot{m}_{oute} + \dot{m}_{outi} - (1-\psi_s)\dot{m}_{ign}] \right.$$
$$+ \frac{(\dot{m}_{ign})^2}{\rho_{g_{LCV}}\pi R_c^2 \phi_{LCV}} - (\dot{m}_{oute}u_{ge})_{LB}$$
$$- (\dot{m}_{outi}u_{gi})_{LB} - N\pi(r_o^2-r_i^2)\Big|_{\xi=-\frac{L}{2}}$$
$$\left. \cdot (\rho_s^2 r_{b_{LB}}/\rho_{g_{LCV}}) - 2\pi R_c Z_L \tau_w \right\} \tag{48}$$
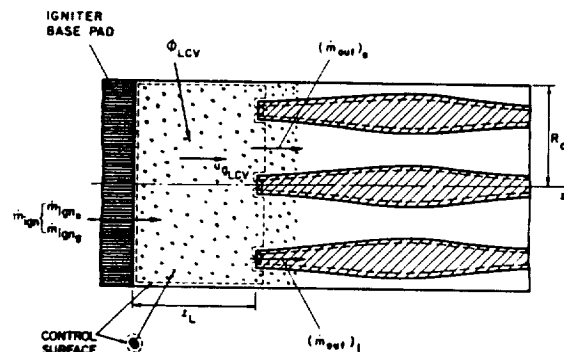

Fig.6 Control Volume Considered for Deriving Governing Equations in the Left Lumped-Parameter Region.

Energy balance:

$$
\frac{dT_{g_{LCV}}}{dt} = \frac{1}{(C_v M_g)_{LCV}} \left\{ C_{v_{LCV}} T_{g_{LCV}} [\dot{m}_{oute} + \dot{m}_{outi} \right.
$$
$$
- (1-\psi_s)\dot{m}_{ign}] + (1-\psi_s)\dot{m}_{ign} C_{p_{LCV}} T_{f_{ign}}
$$
$$
- \dot{m}_{oute}(C_{p_{LB}} T_{ge_{LB}} + u_{ge_{LB}}^2/2)
$$
$$
- \dot{m}_{outi}(C_{p_{LB}} T_{gi_{LB}} + u_{gi_{LB}}^2/2) - \dot{Q}_w 2\pi R_c z_L
$$
$$
\left. - N\pi(r_o-r_i^2) \Big|_{\xi=-L/2} \dot{\rho}_s r_{b_{LB}} C_{pg_{LCV}} T_f \right\} \quad (49)
$$

Equation of state:

$$
P_{LCV} = \frac{R T_{g_{LCV}}}{\dfrac{1}{\rho_{g_{LCV}}} - b} \quad (50)
$$

The void fraction in the left lumped-parameter region, ϕ_{LCV}, can be evaluated from the continuity equation of the condensed-phase products of the igniter which is given as follows.

$$
\frac{d\phi_{LCV}}{dt} = \frac{1}{z_L} \left\{ (1-\phi_{LCV})\left[u_s + r_{b_{LB}} + \frac{\dot{m}_{ign}}{\pi R_c^2 \rho_{ign_s}}\right] - \right.
$$
$$
\frac{\dot{m}_{ign}\psi_s - (1-\phi_{LCV})[\rho_{ign_s} A\phi_{e_{LB}} u_{ge_{LB}} + \rho_{ign_s} N\pi r_i^2 u_{gi_{LB}}]}{\pi R_c^2 \rho_{ign_s}} \right\}
$$

$$(51)$$

The boundary values of velocity, density, pressure, and temperature on the left hand side of both internal and external gas-phase regions can be solved from a number of relationships coupled with Eqs.(44) and (48)-(51). Depending upon the flow directions at left boundary of the internal and external regions, three different cases are identified. In the first case, the flow velocities at stick perforation and the interstitial regions are both in the positive z direction, it can be assumed that the pressure at LCV is equal to those at the left boundary of the stick perforation and the external gas-phase region. Also, the stagnation temperature of the gas in LCV can be assumed to be the same as those on the left boundary. One compatibility relation along the characteristic line in each gas-phase region is used together with the aforementioned equations for solving the flow properties in the LCV and the left boundary.

In the second case, the flow velocity at the left opening if the stick perforation is negative, but the bulk velocity at left boundary of the interstitial void region is still positive. In this case, one additional compatibility relationship can be used for the stick perforation region. Only the pressure at the opening of the stick perforation is considered to be equal to that in the LCV. The treatment for the left boundary of the interstitial

region remains the same as that in the first case.

In the third case, the flow velocities at the left boundray of both the perforation region and the interstitial regions are negative. Therefore, two additional compatibility relationships are available. In this case, both the internal and external gas-phase boundaries are treated in a similar fashion as that for the internal perforation region in the second case.

The void region between the right end of the stick propellants and the projectile base is a lumped-parameter region, which could contain either a base pad with powders of igniter material or an ullage space. In the case of base pad, a set of equations similar to Eqs.(44)-(51) are derived. The right control volume (RCV) is considered to move with the projectile and the left surface of RCV coincides with the right boundary of the stick bundle. A detailed discussion on the compatibility relation mentioned above is given in Ref. 27-28.

H. Empirical Correlations and Constants

Several empirical correlations are used in the model. For the internal gas-phase region, these comprise of the correlations for the burning rate law including erosive burning effect, the convective heat-transfer coefficients, and viscous drag coefficient. The latter two correlations are same as those used in Ref. 15. New erosive burning correlation being developed by authors and coworkers in parallel to this study will be used. For the external gas-phase region, correlations for the convective heat-transfer coefficient, and viscous drag coefficient between the gas-phase and solid surfaces are needed. These correlations are similar to those for the internal perforation region except the fact that they are based on a hydraulic diameter D_H defined as

$$
D_H = \frac{2(R_c^2 - Nr_o^2)}{R_c + Nr_o} \quad (52)
$$

The burning rate law for the external region will be the same as that for the internal perforation region.

For the stick propellants, correlations for F_{pp} and F_{pw}, the ignition criterion, and mechanical and thermal properties are needed. At the present time, not all of this information is available; especially F_{pp} and F_{pw} need to be characterized.

4. Summary of Differences Between the Present and Conventional Formulation

In order to bring out the major differences between the present formulation and the conventional interior ballistic predictive models (4), a summary table is given below.

As summerized by Robbins and Einstein (29), there are differences between the measured and calculated pressures from the NOVA code or its extensions for long unslotted stick propellants. Also, the measured muzzle velocities are higher than those calculated for slotted stick propellants. A number of improvements and considerations suggested in the workshop (29) are incorporated in the present model.

189

Table I

Differences Between the Present Formulation and the
Conventional Interior Ballistic Formulation

Subject under Consideration	Present Formulation	Convential formulation (4)
Typical grain configuration	* Simulation of a number of typical full-length grains in a bundle of stick propellants. * Each stick is modeled as separate tube with deformable and combustible walls.	* Simulation of an average grain in a spatial location along a packed bed of granular propellants. * Each bundle is modeled as a continuum characterized by the velocity and stress in the sticks.
Averaging of flow properties	* The external flow properties are averaged over the cross-sectional flow area of interstitial voids, while the internal flow properties are averaged over the flow area of each stick propellant.	* Flow properties in both external and internal regions are averaged over their respective flow areas.
Grain deformation and fracture	* Simulated by the unbalanced pressure forces between the internal perforation and external interstitial void region. * Linear viscoelastic constitutive law is used. * Employs dynamic finite-element structure mechanics computational code.	* The process of grain deformation and fracture are not addressed, except the longitudinal stresses are considered in the solid-phase momentum equation. * Linear elastic constitutive law is used. * Employs a steady-state relationship between stresses (radial and hoop) and pressures (internal and external)
Grain displacement and acceleration	* The kinematics of the full-length grain is determined from the summation of all forces exerted on the grain.	* The bulk properties of the grains are determined from local momentum balance.
Radiative heat transfer	* Subsurface radiation penetration is allowed and treated by a two-flux model.	* No subsurface radiation penetration is considered.
Type of formulation and frame of reference	* Kinematics and grain deformation are formulated by following the stick (Lagrangian approach) while the gas-phase properties for internal and external regions are determined from a fixed frame of reference (Eulerian approach).	* Both the gas-phase and solid-phase properties are all determined from the conservation equations formulated based upon a fixed frame of reference (Eulerian approach).
Species distribution and location of heat release	* Five groups of species are considered. * Heat release does not have to occur at the site of pyrolysis.	* Gas phase is made of combustion products from ignition and propellant. * Heat release occurs locally at the site of pyrolysis.

Nomenclature

Letter Symbols

a flux model absorption coefficient, m^{-1}

A cross-sectional area of the gun barrel, m^2

A_i preexponential factor of the ith species, m^3/kmol-s

A_p cross-sectional area of the perforation, m^2

A_s specific area of the external surfaces of the stick propellant, m^{-1}

b covolume of the Noble-Abel equation of state, m^3/kg

C_p constant pressure specific heat, J/kg-K

C_s specific heat of stick propellant, J/kg-K

C_v constant volume specific heat, J/kg-K

DR1   group of species pyrolyzed from propellant surface having delayed reactions

DR2   delayed reaction species generated from O and F species

D_v viscous drag force per unit area, N/m^2

D binary diffusion coefficient, m^2/s

e_{ij} deviatoric strain

E total stored energy (internal plus kinetic) per unit mass, J/kg

E_a activation energy, J/kmol

E_b black-body emissive power, $= \sigma T^4$, J/m^2-s

f^k body force per unit volume in k^{th} direction, N/m^3

F fuel rich species pyrolyzed from propellant

F_ξ external force exerted on the solid propellant in the axial direction, N

h specific enthalpy, J/kg

$\bar{h}_c$ convective heat-transfer coefficient, W/m^2-K

h_j specific enthalpy of the jth species, J/kg

h_t total heat-transfer coefficient, W/m^2-K

$\Delta h_{f,i}^0$ standard enthalpy of formation of the ith species, J/kg

I_r outward radiation flux in the positive radial direction, W/m^2

J_r inward radiation flux in the negative radial direction, W/m^2

k thermal conductivity, W/m-K

K bulk modulus of the propellant material, N/m^2

M_g total mass of gas in control volume, kg

M_s instantaneous total mass of a single stick propellant, kg

O oxidizer species pyrolyzed from propellant

P pressure, N/m^2

P final product species

P_b perimeter of the internal perforation, m

$\dot{q}_{rad}$ radiative heat flux per unit time absorbed by the solid propellant surface, W/m^2

$Q_{s_{chem}}$ surface heat release due to pyrolysis, J/kg

$\dot{Q}_w$ rate of heat loss to the tube wall, W/m^2

r_b propellant burning rate, m/s

r_i inner radius of the perforation, m

r_o outer radius of the stick propellant, m

R gas constant, J/kg-K

R_c radius of the combustion chamber, m

R_u universal gas constant, J/kmol-K

s flux-model scattering coefficient, 1/m

S_{ij} deviatoric stress tensor, N/m^2

S surface, m^2

t time, s

T temperature, K

T_f adiabatic flame temperature of the solid propellant, K

u absolute velocity, m/s

V_g gas velocity relative to the solid propellant, m/s

V volume, m^3

W_i molecular weight of the ith species, kg/kmol

x_k coordinate axis in k^{th} direction, m

$\ddot{x}_k$ acceleration in k^{th} direction, m/s^2

$\delta x_{k,m}$ deformation gradient tensor

Y_i mass fraction of ith species, i could represent F, O, DR1, DR2, or P

z axial coordinate in Eulerian coordinate system, m

Greek Symbols

ε_{kk} dilatory strain

ε_s surface emissivity of solid propellant

θ_i angle measured ccw from axis to the tangent to the inner surface of the stick propellant, rad

θ_o angle measured ccw from axis to the tangent to the outer surface of the stick propellant, rad

μ dynamic viscosity of the gas, N-s/m^2

ν_i number of kmoles of ith species

ξ Lagrangian axial coordinate, m

π virtual work, J

ρ density, kg/m^3

σ_{km} Stefan-Boltzmann constant, W/m^2-K^4

σ stress tensor, N/m^2

τ viscous shear stress, N/m^2

τ^k surface traction in k^{th} direction, N/m^2

τ_w tube wall shear stress, N/m^2

$\tau_{\xi\xi}$ normal viscous stress. N/m^2

ψ_s mass fraction of combustion product in the condensed phase from the igniter

$\dot{\omega}_i$ rate of production of ith species, kg/m^3-s

Subscripts

e external interstitial region

g gas-phase, internal or external region

i internal perforation region
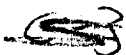
ign igniter
LB left boundary of the stick propellant bundle
LCV left lumped-parameter region in the car-
tridge
RB right boundary of the stick propellant
bundle
s solid propellant or surface

REFERENCES

1. Robbins, F. W., Kudzal, J. A., McWilliams, J.
A., and Gough, P.S., "Experimental Determin-
ation of Stick Charge Flow Resistance, "
Proceedings of the 17th JANNAF Combustion Meet-
ing, CPIA Publication 329, Vol.II, 1980, pp.
97-118.

2. Robbins, F. W., and Horst, A. W., "A Simple
Theoretical Analysis and Experimental Investig-
ation of Burning Processes for Stick
Propellant," Proceedings of the 18th JANNAF
Combustion Meeting, CPIA Publication 347, Vol.
II, 1981, pp. 25-34.

3. Minor, T. C., "Ignition Phenomena in Combusti-
ble-Cased Stick Propellant Charges,"
Proceedings of the 19th JANNAF Combustion Meet-
ing, CPIA Publication 366, Vol. I, 1982, pp.
555-567.

4. Gough, P. S., "Continuum Modeling of Stick
Charge Combustion," Proceedings of the 20th
JANNAF Combustion Meeting, CPIA Publication
383, Vol. I, 1983, pp.351-363.

5. Gough, P. S., "Modeling of Rigidized Gun
Propelling Charges," Contract Report ARBRL-CR-
00518, 1983.

6. Horst, A. W., "A Comparison of Barrel-Heating
Processes for Granular and Stick Propellant
Charges," Memorandum Report ARBRL-MR-03193,
1983.

7. Horst, A. W., Robbins, F. W., and Gough, P. S.,
"Multi-Dimensional, Multiphase Flow Analysis of
Flamespreading in a Stick Propellant Charge,"
Proceedings of the 20th JANNAF Combustion Meet-
ing, CPIA Publication 383, Vol. I, 1983, pp.
365-386.

8. Keller, G. E., "The Competition Between Tube
Heating and Muzzle Velocitiy in Stick Propel-
lant Gun Charges," Proceedings of the 20th
JANNAF Combustion Meeting, CPIA Publication
383, Vol. I, 1983, pp. 387-391.

9. Chiu, D., Grabovsky, A., and Downs, D., "Closed
Vessel Combustion Studies of Stick Propel-
lants," Proceedings of the 20th Combustion
Meeting, CPIA Publication 383, Vol. I, 1983,
pp.393-402.

10. Robbins, F. W., "Continued Study of Stick Pro-
pellant Combustion Processes," Proceedings of
the 19tn JANNAF Combustion Meeting, CPIA Pub-
lication 366, Vol. I, 1982, pp. 443-459.

11. Gough, P. S., "Tne Flow of a Compressible Gas
Through an Aggregate of Mobile, Reacting Part.-
cles," Ph. D. Thesis, McGill University, 1974.

12. Gough, P. S., "The NOVA Code - A User's
Manual," Final Report, Task I, Contract N00174-
79-C-0082, PGA-TR-79-5.

13. Gough, P. S., "Two-Dimensional, Two-Phase Mo-
deling of Multi-Increment Bagged Artillery
Charges," Contract Report ARBRL-CR-00503.

14. Faeth, G. M., "Evaporation and Combustion of
Sprays," Progress in Energy and Combustion Sci-
ence, Vol. 9, 1983, pp. 1-76.

15. Peretz, A., Kuo, K. K., Caveny, L. H., and
Summerfield, M., "The Starting Transient of
Solid-Propellant Rocket Motors With High Inter-
nal Gas Velocities," AIAA Paper No. 72-1119,
Nov.-Dec. 1972.

16. Kuo, K. K., "A Summary of the JANNAF Workshop
on Theoretical Modeling and Experimental Measu-
rements of the Combustion and Fluid Processes
in Gun Propellant Charges," Proceedings of the
13th JANNAF Combustion Meeting, CPIA public-
ation 281, Vol. I, 1976, pp. 213-233.

17. East, J. L., Jr., "Ignition and Flamespreading
Phenomena in Granular Propellant Gun Charges,"
in Interior Ballistics of Guns (H. Krier and M.
Summerfield Eds.), AIAA Progress in Astronau-
tics and Aeronautics, Vol. 66, 1979.

18. Krier, H., and Summerfield, M., Eds., "Interior
Ballistics of Guns," AIAA Progress in Astronau-
tics and Aeronautics, Vol. 66, 1979.

19. Scheidegger, A. E., "The Physics of Flow
Through Porous Media," University of Toronto
Press, 1974, Ch. 6, pp. 123-151.

20. Wu, X., Kumar, M., and Kuo, K. K., "A Compre-
hensive Erosive-burning Model for Double-Base
Propellants in Strong Turbulent Shear Flow,"
Combustion and Flame, Vol. 53, 1983, pp. 49-60.

21. Fifer, R. A., "Chemistry of Nitrate Ester and
Nitramine Propellants," in Fundamentals of
Solid Propellant Combustion (K. K. Kuo and M.
Summerfield Eds.), AIAA Progress Series in As-
tronautics and Aeronautics, Vol. 90, 1984.

22. Kubota, N., "Survey of Rocket Propellants and
Their Combustion Characteristics," in Fundamen-
tals of Solid Propellant Combustion (K. K. Kuo
and M. Summerfield Eds.), AIAA Progress Series
in Astronautics and Aeronautics, Vol. 90, 1984.

23. Spalding, D. B., "Mixing and Chemical Reactions
in Steady Confined Turbulent Flames," Thir-
teenth Symposium (International) on Combustion,
The Combustion Institute, 1965, pp. 1405-1411.

24. GOSMAN, A. D., AND LOCKWOOD, F. C., "Incorpor-
ation of a Flux Model for Radiation into a
Finite-Difference Procedure for Furnace Calcu-
lations," Fourteenth (International) Symposium
on Combustion, The Combustion Institute, 1973,
pp. 661-671.

25. Chang, T. Y., Chang. J. P., Kumar, M., and Kuo,
K. K., "Structural Interaction In a Viscoelas-
tic Material," Research in Nonlinear Structural
and Solid Mechanics, NASA Conference Public-
ation 2147, 1980, pp. 67-90.

26. Key, S. W., Beisinger, Z. E., and Krieg, R. D.,
"HONDO II A Finite Element Computer Program
for the Large Deformation Dynamics Response of
Axisymmetric Solids," Sandia Report SAND78-
0422, 1978.

27. Koo, J. H., and Kuo, K. K., "Transient Combus-
tion in Granular Propellant Beds. Part I :
Theoretical Modeling and numerical Solution of
Transient Combustion Processes in Mobile Granu-
lar Propellant Beds," Final Report, U. S. Army
Research Office , Contract Number
DAAG 29-74-G-0116, 1977.

28. Chen, D. Y., Yang, V., and Kuo. K. K., "Boun-
dary Condition Specification for Mobile

Granular Propellant Bed Combustion Processes,"
AIAA Journal, vol. 19, Number 11, 1981, pp.
1429-1437.

29. Robbins, F., W., and Einstein, S. I., "Workshop
Report: Stick Propellant Combustion Processes,"
to be presented at the 21st JANNAF Combustion
Meeting, Applied Physics Laboratory, Laurel,
MD, Oct. 1-5, 1984.

Editor's Narrative:

Round-Table Discussion: Propulsion Applications of Mixing and
Demixing Processes of Multiphase Flows

Several points were made either explicitly or implicitly in
the presentations and discussions on the second day concerning
mixing processes in multiphase systems and the modeling of these
systems. First, there are situations where transport in turbu-
lent flows can be in a direction other than along the gradient of
the property being transported. This comes about through cou-
pling of density inhomogenieties with pressure gradients, the
former being a consequence of the large temperature differences
in combustion environments. Hence, in turbulent flames, some
transport processes are "counter gradient" or more correctly,
"non-gradient" in nature. Errors due to neglect of these pro-
cesses are not understood, but could possibly be significant in
some combustion systems. Modelers are in the process of learning
to incorporate these ideas into practical codes.

Second, the weakest element in modeling of turbulent multi-
phase flows is probably the turbulence modeling itself. The
treatment of the coupling between the turbulence and the non-
continuously distributed dispersed phase is also a critical area
and includes the question of whether, for numerical purposes, to
treat the dispersed particulate (or droplet) phase as a continuum
or as an assembly of separate particles.

Third, it is possible to treat a very complex problem in great detail by using appropriate levels of approximation and by coupling separate regions together which are best treated with different models or with different levels of approximation.

Fourth, while continuum approaches to multiphase flow calculations are not particularly illuminating in revealing details of the physical processes at work (due to the necessity of averaging quantities before solving the governing equations), there are cases where they can provide useful results for a given problem. The two-fluid approach works best where the dispersed particulate phase is monodisperse, and where the flows are non-reacting.

Sixth, advantages and disadvantages of Favre averaging approaches were discussed. An advantage is that the conservation equations for variable density with Favre averaging are much like the standard constant density equations. Disadvantages are that there is some difficulty in obtaining molecular terms and computed and measured quantities are more difficult to compare.

Finally, physical situations for which multiphase flow models are appropriate generally contain a very broad range of length and time scales within the same problem. This means that when computational approaches to these problems are used, some levels of approximation will need to be made in order to deal with these large ranges of scale. The point in the analysis at which approximation is made is a key difference between a two-fluid model and an Eulerian-Lagrangian model of a dispersed particulate phase in a fluid phase.

1. REPORT NO. NASA CP-3006	2. GOVERNMENT ACCESSION NO.	3. RECIPIENT'S CATALOG NO.
4. TITLE AND SUBTITLE Mixing and Demixing Processes in Multiphase Flows With Application to Propulsion Systems		5. REPORT DATE July 1988
		6. PERFORMING ORGANIZATION CODE
7. AUTHOR(S) Edited by Rand Decker* and Charles F. Schafer		8. PERFORMING ORGANIZATION REPORT #
9. PERFORMING ORGANIZATION NAME AND ADDRESS George C. Marshall Space Flight Center Marshall Space Flight Center, Alabama 35812		10. WORK UNIT NO. M-591
		11. CONTRACT OR GRANT NO.
		13. TYPE OF REPORT & PERIOD COVERED
12. SPONSORING AGENCY NAME AND ADDRESS National Aeronautics and Space Administration Washington, D.C. 20546		Conference Publication
		14. SPONSORING AGENCY CODE

15. SUPPLEMENTARY NOTES

Prepared by Structures and Dynamics Laboratory, Science and Engineering Directorate.

*NRC Associate

16. ABSTRACT

A workshop on transport processes in multiphase flows was held at the Marshall Space Flight Center on February 25 and 26, 1988. This document provides the program, abstracts, and text of the presentations made at this workshop. In addition, the content of two open discussion sessions are presented in narrative form. The objective of the workshop was to enhance our understanding of mass, momentum, and energy transport processes in laminar and turbulent multiphase shear flows in combustion and propulsion environments.

17. KEY WORDS Multiphase Flow, Transport Processes, Turbulence, Continuum Models, Lagrangian-Eulerian Models, Drag, Lift, Particle Migration	18. DISTRIBUTION STATEMENT Unclassified – Unlimited Subject Category: 34
19. SECURITY CLASSIF. (of this report) Unclassified	20. SECURITY CLASSIF. (of this page) Unclassified	21. NO. OF PAGES 202	22. PRICE A10